



Effect of Cosolvents on the Phase Separation of Polyelectrolyte Complexes

Journal:	<i>Soft Matter</i>
Manuscript ID	SM-ART-07-2024-000903.R1
Article Type:	Paper
Date Submitted by the Author:	26-Aug-2024
Complete List of Authors:	<p>Ma, Yuanchi; Qingdao University of Science and Technology, Ivancic, Robert; National Institute of Standards and Technology, Materials Science and Engineering Division, Material Measurement Laboratory</p> <p>Obrzut, Jan; National Institute of Standards and Technology, Materials Science and Engineering Division, Material Measurement Laboratory</p> <p>Audus, Debra; National Institute of Standards and Technology Materials Science and Engineering Division, Materials Science and Engineering Division</p> <p>Prabhu, Vivek; National Institute of Standards and Technology, Materials Science and Engineering Division, Material Measurement Laboratory</p>

ARTICLE

Effect of Cosolvents on the Phase Separation of Polyelectrolyte Complexes

Yuanchi Ma^{a,*}, Robert J. S. Ivancic^b, Jan Obrzut^b, Debra J. Audus^b, Vivek M. Prabhu^{b,*}

Received 00th January 20xx,
Accepted 00th January 20xx

DOI: 10.1039/x0xx00000x

ABSTRACT: Evidence is shown that cosolvent mixtures control the coacervation of mixtures of oppositely charged polyelectrolytes. Binary and ternary solvent mixtures lead to non-monotonic solubility as a function of the average dielectric constants of the solvent mixtures. These data are rationalized by considering both electrostatic-driven and solvophobic-driven phase separation using group contribution effects on solubility parameters. These estimates are introduced into an effective Flory-Huggins interaction parameter within the framework of Voorn-Overbeek theory with variable dielectric constant and temperature dependences. Despite its simplicity, the model recovers salient experimental observations not only on the coacervate stabilities, but also on their lower-critical solution temperature behaviors. These observations highlight the importance of the weak van der Waals interactions in determining the phase behaviors of polyelectrolyte complexes relative to the electrostatic correlations.

Introduction

Associative phase separation is a common phenomenon in polyelectrolyte complexes (PECs), whereby oppositely charged polyelectrolytes separate into solvent-rich supernatant phases and polymer-rich coacervate phases. Despite their broad applications in adhesives^{1,2}, structured membranes, coatings³ and therapeutic delivery vehicles⁴, a comprehensive physical picture of PECs remains to be elucidated. The convolution between the long-range electrostatic and van der Waals interactions in multicomponent systems adds to the challenge to model experimental data⁵. The relative significance of these two classes of interactions are debated across a variety of systems, including ionic fluids^{6–8}, polyelectrolyte brushes^{9,10}, and intrinsically disordered proteins¹¹. In PECs, the role of charge correlation is increasingly invoked as a major contributor to phase separation¹², where the complexation of polyelectrolytes and the concomitant counterion release are driving forces^{13,14}. Nonetheless in the literature, polyelectrolyte complexes have hitherto been discussed almost exclusively in aqueous media, whereas experiments and theories on PECs in binary and more complicated solvent mixtures are largely unexplored.

Similar to neutral polymer solutions, polyelectrolyte complex solutions also display unique critical temperature behaviors^{15–17}. Their net temperature dependences are governed primarily by the static dielectric constant (ϵ_0) and an

effective Flory-Huggins parameter (χ). The former is embodied within the Bjerrum length (l_B) that equates the thermal energy to the Coulombic potential energy between charges separated through a medium of dielectric constant. The latter is the sum of all enthalpic contributions to the mixing free energy, arising from the weak van der Waals interactions between nearest neighbors, such as monomers and solvent molecules, often referred to as the “solvophobic” contribution. It was reported that synthetic PECs in aqueous solution primarily display lower critical solution temperature (LCST) behavior^{18,19}, whereas upper-critical solution temperature (UCST)²⁰ is occasionally observed. Such critical temperature dependences were successfully modelled by Adhikari et al.^{21,22} using the combinations of a realistic temperature (T) dependencies of ϵ_0 and two empirical $\chi(T)$ functions to differentiate electrostatic and the solvophobic contributions to the phase separation of PECs. Notably in their computation, LCST, UCST as well as both LCST and UCST behaviors are predicted depending on the exact parameterization, suggesting complexity of such systems. Similarly, Ylitalo et al.²³ showed that the LCST was electrostatic in origin by considering the temperature dependence of the dielectric constant in a liquid state theory.

On the experimental side, effort has been made to deconvolute the effect of Coulombic interactions and van der Waals interactions on the coacervation of PEC solutions. Li et al. systematically studied two PECs with nearly identical charge density but distinct backbone-solvent interactions: the hydrophobic pair comprises of sodium poly(acrylate) (PAA) and poly(allylamine hydrochloride) (PAH) with aliphatic backbones, while the hydrophilic pair comprises of sodium poly(glutamate) (PRE) and poly(L-lysine hydrochloride) (PLK) with peptide backbones. The former was shown to phase-separate more readily than the cross-paired PAA + PLK and PRE + PAH, than the latter.²⁴ In an earlier study, Lou et al. started with a pair of

^a College of Polymer Science and Engineering, Qingdao University of Science and Technology, Qingdao, Shandong, China.

^b Materials Science and Engineering Division, Material Measurement Laboratory, National Institute of Standards and Technology, 100 Bureau Drive, Gaithersburg, MD, United States.

Electronic Supplementary Information (ESI) available: [details of any supplementary information available should be included here]. See DOI: 10.1039/x0xx00000x

hydrophobic, sulfide-containing poly(sulfonate) and poly(amine hydrochloride), and applied different oxidation level to tune the backbone-solvent interactions while keeping the charge density nearly constant. They observed a clear downshift of the salt-dependent, not temperature dependent, binodal phase envelopes with increasing oxidation level (i.e., backbone hydrophilicity).²⁵ Despite the chemical difference of PECs, both authors reported enhanced miscibility of the complexes when the backbone-solvent (water) interaction becomes more favorable, reminiscent of the phase behavior of simple binary mixtures of neutral polymers and solvents in the spirit of Flory-Huggins theory. Considering these previous studies, we sought to push our understandings one step further by keeping the PEC backbones constant while investigating the effect of varied solvent compositions to the phase behavior of PECs, where ϵ_0 and χ simultaneously changed by solvent compositions in a non-trivial way.

Potassium poly(styrene sulfonate) (KPSS) and poly(diallyldimethylammonium) bromide (PDADMAB) are two water soluble polyelectrolytes, while their complexation results in phase-separation under ambient temperature and low-salt conditions. With the charge stoichiometry of 1:1, the transition of this complex solution from two-phases to one-phase takes place at approximately 1.8 mol/L of added KBr, defined as the salt resistance, or the threshold salt concentration ($c_{s,th}$)^{19,26,27}. As $c_{s,th}$ depends on the total polyelectrolyte concentration^{18,19} (c_p), it is therefore facile to use $c_{s,th}$ at a given c_p as the proxy for the height of the two-phase window in the entire phase diagram. This strategy was employed previously^{28–31} as a simple and intelligible way to report the phase behaviors of a variety of polyelectrolyte complex solutions. In this study, we fixed $c_p = 0.10$ mol/L and $T = 20$ °C, while varying the volume fraction of cosolvents and the total salt concentration ($c_s = c_{s,added} + c_{s,counterion}$) progressively to determine the $c_{s,th}$ for each solvent composition. We selected ethylene glycol (EG) and N-methylformamide (NMF) as the cosolvents, as they are both miscible with water, and have moderate solubilities to the two polyelectrolytes and the salt (KBr). Furthermore, pure EG has a lower static dielectric constant ($\epsilon_{EG} = 38$) than water ($\epsilon_{H_2O} = 80$) at room temperature, characteristic to most organic solvents with small dipole moments, while pure NMF has a much higher static dielectric constant ($\epsilon_{NMF} = 187$) partially due to the presence of directional hydrogen bonds^{32,33}. Therefore, mixing EG or NMF with water allows for the tuning a wide range of static dielectric constant and consequently the strength of electrostatic interactions. Previous fundamental research on the temperature-dependence of low ionic strength polyelectrolytes in NMF solutions were the first to study the effect of varied Bjerrum length on the dynamics^{34–36}.

bound of the cosolvents are restricted by the solubility of the polyelectrolytes and KBr, therefore the regions of $\phi_{EG}^S + \phi_{NMF}^S > 0.5$ were not further pursued. We conducted broadband dielectric spectroscopy measurements to determine the ϵ_0 of each solvent mixture (see experimental and Section I of Electronic Supplementary Information (ESI) for more details). These measurements agree with the literature values^{32,33,37}. By plotting the data in Table 1 with $c_{s,th}$ against ϵ_0 (as shown in Figure 1a), for the binary solvent mixtures (EG + H₂O in blue and NMF + H₂O in red), $c_{s,th}$ do not show a monotonic dependence on ϵ_0 , but display a sharp maximum at $\epsilon_0 = 80$ (the black symbol), corresponding to the case of water. From the perspective of solvent composition, most of the variance in $c_{s,th}$ can be qualitatively explained by the volume fraction of water ($\phi_{H_2O}^S$), regardless of the direction of ϵ_0 . A similar trend is evident in ternary solvent mixtures with varying $\phi_{H_2O}^S$ and constant ratio of ϕ_{EG}^S/ϕ_{NMF}^S (the green symbols). On the high dielectric constant branch (NMF + H₂O), this trend is expected because the strength of electrostatic interaction decreases with ϵ_0 , leading to the enhanced stability of soluble complexes, and therefore lower salt concentration required to homogenize the system. On the low dielectric constant branch (EG + H₂O), however, we note that the decreased $c_{s,th}$ at lower ϵ_0 (or higher Bjerrum length l_b) is in contrast with predictions by Zhang et al. using a χ -free model based on liquid-state theory³⁸, but in agreement with a recent experimental work by Meng et al.³⁹, who also observed decreased $c_{s,th}$ for PSS-PVBtMA [Poly(vinylbenzyl) trimethylammonium chloride] complexes at lower dielectric conditions in water-ethanol mixtures, where the static dielectric constant of ethanol is 24.5. These strongly suggest the importance of invoking an effective χ to account for the discrepancy between theories and experiments.

Table 1. $c_{s,th}$ of KPSS-PDADMAB complexes in solvent mixtures at $c_p = 0.10$ mol/L.

Solvent	$\phi_{H_2O}^S$	ϕ_{EG}^S	ϕ_{NMF}^S	ϵ_0 ^a	$c_{s,th}$ [mol/L]
H ₂ O	1.00	0	0	80.0	1.80 ± 0.01
Binary: H ₂ O/EG	0.90	0.10	0	76.8	1.59 ± 0.01
	0.75	0.25	0	71.6	1.35 ± 0.01
	0.60	0.40	0	66.5	1.14 ± 0.01
	0.50	0.50	0	62.7	1.10 ± 0.01
Binary: H ₂ O/NMF	0.90	0	0.10	83.2	1.41 ± 0.01
	0.75	0	0.25	88.0	1.20 ± 0.01
	0.60	0	0.40	95.3	1.05 ± 0.01
	0.50	0	0.50	102.1	1.00 ± 0.01
Ternary: H ₂ O/EG/NMF	0.90	0.072	0.028	78 ± 1 ^b	1.52 ± 0.01
	0.75	0.18	0.07	75.0	1.27 ± 0.01
	0.60	0.288	0.112	70 ± 1 ^b	1.09 ± 0.01
	0.50	0.36	0.14	68.0	1.05 ± 0.01

Notes: (a) Measured by dielectric spectroscopy. (b) Calculated by interpolation of the experimental data.

Results and discussion

Phase Behavior of PECs at Various Solvent Compositions

The phase behavior of the KPSS-PDADMAB complexes were investigated in binary and ternary solvent mixtures of H₂O with EG and NMF for cosolvent volume fractions relative to the solvent volume (ϕ_{EG}^S , ϕ_{NMF}^S) up to 0.50 (Table 1). The upper

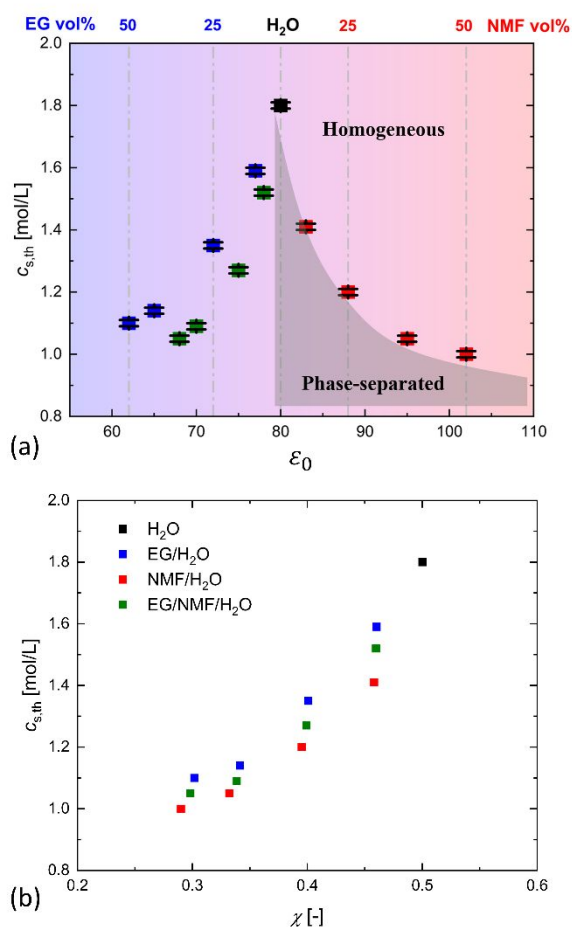


Figure 1. (a) $c_{s,th}$ of KPSS-PDADMA complexes as a function of ϵ_0 (bottom axis). The blue and red symbols represent the binary mixtures of EG + H₂O and NMF + H₂O, respectively; the green symbols represent the ternary mixtures. The dash-dotted lines indicate the solvent compositions (top axis) and the grey-shaded area reminds readers of the phase-separated nature of PECs in the low-salt regime. These marks are for visual aid only. (b) The same data in (a) plotted as a function of χ_{avg} (see Table 2 and related narrative for details). Uncertainties were not estimated for values of χ .

By its strict definition, χ of a binary mixture should only reflect the overall *local* enthalpic interactions. In multicomponent ion containing systems such as polyelectrolyte and PEC solutions the solution may require multiple χ to account for all pair-wise interactions or an effective χ that assumes a lumped contribution. Therefore in the present study, we seek to estimate the χ between solvents and polyelectrolytes ($\chi_{\text{solvent-p}}$) through the group contribution theory based on Hansen solubility parameters^{40,41}, a classical approach to predict the miscibility of neutral compounds. The equivalent uncharged structures for PSS[−] and PDADMA⁺ are proposed in Scheme S1, and a short account of this approach is given in the ESI. The results of these calculations are given in Table 2. These values are computed with respect to the reference volume $l^3 = 0.0366 \text{ nm}^3$ and scaled to provide reasonable agreement between our theoretical model and experimental results. While the scaling parameter is somewhat less than the optimal one found in Ref. 42, we note that much of the previous study's data was fit to poly(butyl methacrylate)

and poly(vinyl acetate). On average, the Flory-Huggins parameters between the pure solvents and the equivalent polyelectrolyte pairs, *i.e.*, $\chi_{\text{H}_2\text{O-p}}$, $\chi_{\text{EG-p}}$ and $\chi_{\text{NMF-p}}$ are 0.50, 0.10 and 0.080, respectively. These values are estimates of the charge-deconvoluted solvent-polymer interactions: as both the polyanion and polycation have hydrophobic backbones, their solvent selectivity should follow the order of increasing hydrophobicity, *i.e.*, $\text{H}_2\text{O} < \text{EG} < \text{NMF}$, which naturally leads to $\chi_{\text{H}_2\text{O-p}} > \chi_{\text{EG-p}} > \chi_{\text{NMF-p}}$. Figure 1b shows the same $c_{s,th}$ data plotted against the average χ (χ_{avg}), where we assume the interaction between solvent mixtures and polymers are volume-weighted averages of individual solvent-polymer interactions, *i.e.*, $\chi_{\text{avg}} = \phi_{\text{H}_2\text{O}} \chi_{\text{H}_2\text{O-p}} + \phi_{\text{EG}} \chi_{\text{EG-p}} + \phi_{\text{NMF}} \chi_{\text{NMF-p}}$. The sharp maximum of $c_{s,th}$ in Figure 1a can now be reasonably explained by the highest χ reflecting water-polymer interactions. In a related study, Li *et al.* compared the phase separation conditions²⁴ of two pairs of PECs with hydrophilic backbones (amide) and hydrophobic backbones (vinyl), and found that the latter has a $c_{s,th}$ at least 6 times as large as the former in water. Their study, though tuning the polymer-solvent interaction through a different approach, also underpinned the vital role of χ in dictating the associative phase separation of PEC.

Similarly, Lou *et al.* in a series of homologous PECs with identical backbones and a judicious combination of sulfide, sulfone and sulfoxide groups next to cations and anions, which are designed to examine the effect of local polarity on the phase behavior of PECs.²⁵ Using a sophisticated model, the authors observed χ values that progressively decrease with increasing molecular polarity (*i.e.*, better hydrophilicity) as extracted by fits to experimental binodal phase diagrams. Notably, their χ values obtained from fitting are largely in accord with estimated values in Table 2, perhaps lending some credence to estimates based on solubility parameters.

Table 2. Calculated effective $\chi_{\text{solvent-p}}$ values at room temperature.

$\chi_{\text{solvent-p}}$	H ₂ O	EG	NMF
PSS	0.41	0.078	0.058
PDADMA	0.59	0.13	0.10
Average	0.50	0.10	0.080

Application of the Voorn-Overbeek Theory

In order to discern the source of the reduction of the critical salt concentration with decreasing H₂O, we use the Voorn-Overbeek (VO) theory.⁴³ While this model does not account for counterion binding, polymer connectivity, or dipole interactions, it allows us to determine if non-electrostatic interactions are primarily responsible for the non-monotonic behaviour. In VO theory, the single phase free energy density (f) of PEC solutions is

$$\frac{l^3 f(\phi_p, \phi_s)}{v k T} = \frac{\phi_p}{N} \ln \left(\frac{\phi_p}{2} \right) + \phi_s \ln \left(\frac{\phi_s}{2} \right) + \phi_0 \ln \phi_0 + \chi \phi_p \phi_0 - \alpha (\phi_s + \sigma \phi_p)^{\frac{3}{2}} \quad (1)$$

In this equation, the first three terms represent the entropy of mixing of polymer, salt, and solvent. The fourth term represents the enthalpy of mixing from Flory-Huggins theory, and the last term represents the Debye-Hückel approximation of total

electrostatic free energy introduced by all charged moieties. Here φ_i is the volume fraction of component i , l is the lattice size, V is the system volume, k is Boltzmann's constant, T is temperature, and N is the reduced chain length. The strength of the electrostatic interactions is determined by $\alpha = (2\sqrt{\pi}/3)(l_B/l)^{3/2}$, in which $l_B = e^2/4\pi\epsilon_0\epsilon_0 kT$ is the Bjerrum length with elementary charge (e) and permittivity of free space (ϵ_0). The charge density (σ) equals the total polymer charge divided by N . To reduce complexity, polymers, salts, and solvents are each treated as a single species. In the case of the solvents, this is equivalent to assuming the relative volume fractions of the three solvents is the same in both phases. This assumption is reasonable given that the data in Fig. 1b nearly collapses on a single curve.

To apply this model, we use microscopic data from the experiments for parameterization rather than fitting the model to the experimental data. Therefore, the results are based on the model's underlying physics rather than its ability to fit the data. We define l as the size of a water molecule (0.332 nm). We take $N = 1000$ and $\sigma = 0.1$ commensurate with the polymers. The values χ and ϵ_0 are the same as those used in Figure 1b. Additional details of model parameterization can be found in the Section III of ESI.

The coexistence curves on the φ_s - φ_p (c_s - c_p) plane were obtained by minimizing the total free energy, with the results shown in Figure 2a. As anticipated, all the phase boundaries have similar shapes. The theoretical $c_{s,th}$ at $c_p = 0.10$ mol/L are extracted from Figure 2a via the intersection of the dashed line and the phase boundaries. These values are plotted in Figure 2b together with the experimental $c_{s,th}$ for direct comparison. As can be seen in Figure 2b, the VO theory semiquantitatively reproduces the experimental trend of $c_{s,th}$ vs ϵ_0 with a minimal set of microscopically defined parameters. To determine how non-electrostatic interactions affect this prediction, we also fix χ to be that of H₂O and vary ϵ_0 . As can be seen in Figure 2b, this results in a monotonic dependence of $c_{s,th}$ on ϵ_0 .

The agreement between experimental data and VO theory combined with the monotonic result once χ was fixed suggests that non-electrostatic interactions are primarily responsible for the non-monotonic behaviour in $c_{s,th}$. This result indicates that including counterion binding, connectivity of the polymer in electrostatics, dipolar interactions, preferential solvation,^{44,45} local dielectric constants,^{46–48} varying χ as a function of φ_p ,⁴⁹ and treating each species independently^{50–52} are not necessary to understand the source of non-monotonicity. However, use of a more advanced theory^{53,54,38,21,25,23,55}, to explore varying χ but not varying ϵ_0 , may be able to elevate the predictions from semiquantitative to fully quantitative, especially the plateauing of $c_{s,th}$ with increasing φ_{NMF} . Small-angle neutron scattering combined with a multicomponent random phase approximation theory was used to extract the three Flory-Huggins parameters among polymer and two solvents by Jia et al on an LCST systems.^{56,57} Such an approach within an appropriate theory may test the assumption of χ weighted by the cosolvent volume fraction.

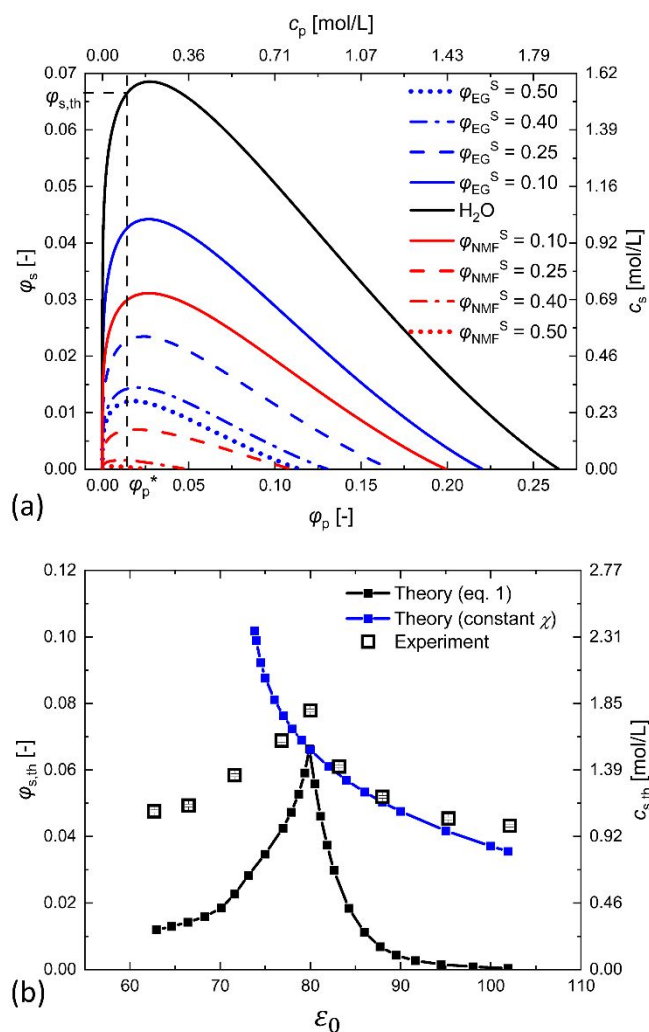


Figure 2. (a) Theoretical φ_s - φ_p phase diagrams calculated by VO theory in various solvent compositions. The c_s axis is associated with the φ_s by $c_s = \varphi_s \rho_s / M_s$, and the c_p axis is associated with the φ_p by $c_p = \varphi_p \rho_p / M_p$, where ρ and M are the density and molecular weight. Here we use $\rho_s = 2.75$ g/mL and $M_s = 119$ g/mol for KBr, and $\rho_p = 1.1$ g/mL and $M_p = 154$ g/mol to estimate the average of a PSS-PDADMA monomer pair with 1:1 stoichiometry. The vertical dashed line indicates the experimental c_p of 0.10 mol/L, and its intersections with the coexistence curves define the theoretical $\varphi_{s,th}$ or $c_{s,th}$. (b) Comparison between theoretical and experimental $c_{s,th}$ at $c_p = 0.10$ mol/L, plotted as a function of ϵ_0 . Uncertainties in the measurement are provided in Table 1 and are typically smaller than the symbols.

Effect of Solvent Mixture on Lower Critical Solution Temperature

Figure 3 shows the representative transmittance- T curves of the KPSS-PDADMA complex solutions in binary and ternary solvent mixtures. In all samples, liquid-liquid phase separation was observed upon heating, as evident by the drastic decrease in transmission. Such a universal LCST behavior across the entire solvent range^{18,19,27} is likely driven by the stronger electrostatic interaction at higher T , embodied in the $l_B(T)$ of water, EG and NMF as increasing functions of T (Figure S5). The temperature dependence of the hydrophobic interaction between polyelectrolytes and solvents as represented by $\chi(T)$, on the other hand, has so far been poorly understood. Here we introduced an empirical χ expression that includes both the enthalpic and entropic contributions following the formalism of the Flory-Huggins theory, i.e., $\chi(T) = \chi_H/T + \chi_S$, and our simple

model is able to capture an increase in critical salt concentration with increasing temperature through judicious parameterization of χ_H and χ_S , which is consistent with the LCST behavior of PEC solutions up to 50 % cosolvent volume fraction (as shown in Figure S8, using $\chi_S \approx 4\chi_H/(293\text{ K})$ as an example). Decreasing the entropic contribution of $\chi(T)$, however, can result in the reverse of the modelling results to UCST behaviors, due to the overwhelming miscibility of polyelectrolytes and solvents at high temperature (as shown in Figure S9, using $\chi_S = 0$ as an example). In the work by Adhikari et al.²², multiple phase behavior scenarios were also reported in aqueous PEC solutions, whereas in the present case, the trend based upon the solvent mixtures is highlighted. The sensitivity in the choice of parameters (χ_H vs χ_S) reflects the complexity of these PEC systems, and suggests the electrostatic-solvophobic competition as a possible mean-field mechanism for the dual miscibility gaps observed by Ye et al.²⁰ and predicted by Adhikari et al.²² It is worth mentioning that the current knowledge on the criticalities of synthetic PECs are so far mostly established on the (Na/K)PSS-PDADMA(Cl/Br) systems and may therefore only stand for the case of hydrophobic backbones. From this sense, a systematic study of the temperature dependence of other model PEC systems of intermediate²⁵ or high backbone hydrophilicity²⁴ (and preferably, with low molar mass dispersity) would be beneficial to provide a general picture on this long-standing issue.

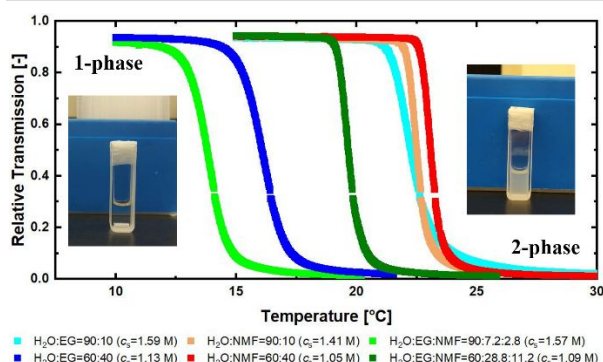


Figure 3. Representative transmittance curves of KPSS-PDADMA complexes in binary EG/H₂O, NMF/H₂O and ternary EG/NMF/H₂O mixtures with $c_p = 0.10$ mol/L and $c_s \approx c_{s,thr}$ nearly identical to the conditions listed in Table 1. The inset figures are representative photographs of the same PEC solution in a DLS glass cuvette prior to (at low temperature) and after (above the LCST) phase separation.

Apart from the temperature criticality and the phase diagrams^{18,19}, we have also shown in our earlier study that upon approaching the critical temperatures, polycations and polyanions strongly associate with each other in water and eventually lead to concentration fluctuations of sub-micron size at incipient phase separation^{19,27}. Therefore, it is also of interest to investigate whether such chain association in mixed solvents is comparable with that in aqueous solution, or does it introduce new structures detectable by dynamic light scattering (DLS). Figure 4 illustrates the trends in equivalent hydrodynamic radii ($R_{h,eq}$) of the polyelectrolyte chain associates at various c_p with temperature in the case of binary EG/H₂O cosolvent with $\varphi_{EG}^S = 0.5$. The horizontal axis here is $(T_{cp}-T)/T_{cp}$ rather than T for the purpose of direct comparison between the data, where T_{cp} is the cloud point temperature of each individual sample as

defined by the inflection points of transmittance- T curves in Figure 3. Therefore, the dimensionless $(T_{cp}-T)/T_{cp}$ denotes the thermodynamic distance of the experimental temperature to the phase separation temperature, nearly identical to the formalism of the Ginzburg criterion that is typically used to describe phase-separating charge-neutral systems. The polymer concentrations of 0.05 mol/L to 0.30 mol/L were selected to cover from dilute to semidilute solutions. Here for clarity, we discuss the size of solution structures in the context of equivalent hydrodynamic radii, $R_{h,eq}$, while keeping in mind that the classical Stokes-Einstein relationship of $R_h = kT/6\pi\eta_0D$ is only strictly valid in dilute solutions where all interparticle interactions are negligible with solvent viscosity, η_0 ²⁷. Moreover, at temperatures that are sufficiently close to T_{cp} , the measured diffusion coefficients (D) given by DLS no longer represent the diffusion coefficients of individual particles or clusters, but instead the collective diffusion coefficients of concentration fluctuation modes as predicted by the mode-coupling theory⁵⁸. This is beyond the scope of this paper but was addressed elsewhere.²⁷ Here we do not distinguish the difference between the two but refer to the structures indiscriminately as associates. As can be clearly seen in Figure 4, under all cases, the evolution of the chain association states in EG/H₂O (red symbols and lines) display striking similarities to that in pure water (black symbols and lines), with nearly overlapping curves for $c_p = 0.2$ mol/L and 0.3 mol/L, and only minor deviations for $c_p = 0.05$ mol/L and 0.1 mol/L within experimental uncertainties on the logarithmic scale. Our results suggest that the effect of cosolvents does not change the dynamics of polyelectrolyte complexes, but only renormalizes their threshold salt concentrations and critical temperatures of phase separation.

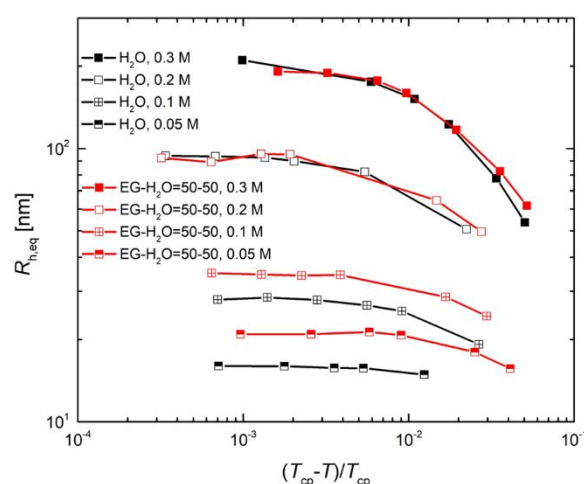


Figure 4. Equivalent hydrodynamic radii ($R_{h,eq}$) of the polyelectrolyte complex aggregates in EG/H₂O=50/50 and pure water as a function of the thermodynamic distance, $(T_{cp}-T)/T_{cp}$. The solid lines connecting the data points are for visual aid. Uncertainties (error bars) are within the size of the symbols used and not shown, but were estimated by one standard deviation from the model fit to determine the diffusion coefficient and propagated to estimate the hydrodynamic radius using the Stokes-Einstein relation.

Conclusions

In conclusion, we observed strong influence of cosolvents on the phase behaviour of KPSS/PDADMA complexes, which displays a non-monotonic dependence on the average dielectric constants of the binary or ternary solvent mixtures but can be reasonably interpreted by invoking a solvent-polymer backbone interaction term. The phase envelope shifts as a function of the cosolvent compositions were semiquantitatively captured by the VO model. While we expect that adding additional detail would lead to more quantitative results, the simplicity of this model allows for a direct comparison of the importance of the electrostatic and non-electrostatic effects in describing this phenomenon. This model indicates that the van der Waals interactions are key to understanding the phase stability of coacervates in accord with our experimental findings. Moreover, within the broad composition window of cosolvents (EG-H₂O-NMF) used in this study, all PEC solutions manifest a universal LCST criticality, which is consistent with previous findings^{18,19,27} and captured by the VO model as well by judicious parameterization. Further light scattering measurements lend credence on the similarity of the near-critical dynamics of PECs in aqueous and solvent mixtures. In all, our findings imply a novel way of tuning the phase stability of PEC solutions and may motivate fundamental studies in the fields such as biomedicines and cryo-preservation of cells, which also deal with similar circumstances where cosolvents are introduced to ensure solubility or proper functioning of proteins under harsh environments or processing conditions.

Experimental

Materials and Polyelectrolyte complex sample preparation*

Ethylene glycol (Fisher Scientific, certified grade) and N-methylformamide (Sigma-Aldrich, 99 % purity) were used as received. Sodium poly(styrene sulfonate) (Sigma-Aldrich, nominal molar mass ≈ 200 kg/mol, 30 % by mass fraction in H₂O) and poly(diallyl dimethylammonium chloride) (Sigma-Aldrich, nominal molar mass $\approx (100 \text{ to } 200)$ kg/mol, 20 % by mass fraction in H₂O) were purified and counterion exchanged by previously reported methods. The number-average relative molar masses (M_n), dispersity (\mathcal{D}), and degree of polymerization (DP) are summarized in Table 3.

Table 3. Characteristics of KPSS and PDADMA

Polyelectrolytes	M_n (kg/mol)	\mathcal{D}	DP
KPSS	70 ^a	2.80	315
PDADMA	22 ^b	2.76	107

Note: (a) relative number average molar mass determined by size exclusion chromatography (SEC) using NaPSS as calibrants; (b) relative number average molar mass determined by SEC using poly(vinylpyrrolidone) as calibrants.

The dry KPSS and PDADMA were individually dissolved in mixed solvents with predetermined ratio of milli-Q water, EG and NMF to prepare 0.50 mol/L polymer stock solutions. The 2.00 mol/L stock solutions or KBr were similarly prepared. The stock solutions of KPSS, PDADMA and KBr were mixed with their corresponding blank solvents to prepare polyelectrolyte

complex solutions with various salt concentrations (c_s). These complex solutions were vortex-mixed and vigorously agitated to ensure complete mixing and stored in fridge at 5 °C to avoid solvent evaporation. The statuses of phase separation of the samples were determined by laser light transmittance measurement, with 50 % transmittance as a criterion to distinguish between homogeneous and phase-separated.

Dielectric measurements

Materials. Anhydrous NMF and EG were obtained from Sigma Aldrich and used without further purification. Ultrapure water with resistance reading > 25 M Ω was purified by a laboratory filtration and deionization unit. Concentration of mixtures was determined gravimetrically by weighing content of pure components using a microbalance and then normalizing the mass fraction to volume fraction using specific density of water (1.00 g/cm³), NMF (1.110 g/cm³) and of EG (1.010 g/cm³) respectively.

Methods. The static dielectric constant, ϵ_0 , of pure solvents and their mixtures was determined from the measurements of complex dielectric permittivity ($\epsilon^* = \epsilon' - j\epsilon''$) performed at 23 °C in a broadband frequency range, from 400 MHz to 20 GHz. The measurements were performed using the Agilent 8720D Vector Network Analyzer and Agilent 8570E Dielectric Probe Kit with an open-ended coaxial probe. The probe was impedance calibrated to Open, Short and Water microwave impedance standards in accordance with the manufacturer specification for 8570E.

The example of experimental data of $\epsilon''(\omega)$ and $\epsilon'(\omega)$ measured for NMF-H₂O mixtures are plotted in Fig. 5a on the Cole-Cole ϵ'' vs. ϵ' complex plane, where angular frequency (ω) is the independent parameter.

At higher frequencies, above 15 GHz, in the range where $\epsilon'(\omega) < 40$ (Fig. 5a), the experimental ϵ'' and ϵ' data are somewhat scattered due to effects of multiple reflections resulting from the dielectric compression of microwaves wavelength propagating in the high dielectric constant media. The plots in Fig. 5a show apparent shape of Cole-Cole semi-circles that intersect $\epsilon'(\omega)$ axis when $\epsilon''(\omega) = 0$. The two intersection points give the value of unrelaxed dielectric constant, $\epsilon_\infty(\omega \rightarrow \infty)$ and the static dielectric constant, $\epsilon_0(\omega \rightarrow 0)$, which are parameters of the Cole-Cole relaxation model⁵⁹.

In order to determine ϵ_0 from our empirical data we can assume the single dielectric relaxation model of Debye for $\epsilon''(\omega)$ ⁵⁹ described by,

$$\epsilon''(\omega) = \frac{(\epsilon_0 - \epsilon_\infty)\omega\tau}{1 + \omega^2\tau^2} \quad (2)$$

where, ω is the angular frequency, $\epsilon''(\omega)$ is the imaginary part of the dielectric permittivity, and τ is the relaxation time.

Equation (2) can be rearranged into (3):

$$\omega\epsilon''(\omega) = \frac{1}{\tau}(\epsilon_0 - \epsilon'(\omega)) \quad (3)$$

which represents a linear relation between the measured $\epsilon''(\omega)$ and $\epsilon'(\omega)$. The static dielectric constant, ϵ_0 , is derived from (3) as the intercept of a straight line with the slope of $1/\tau$.

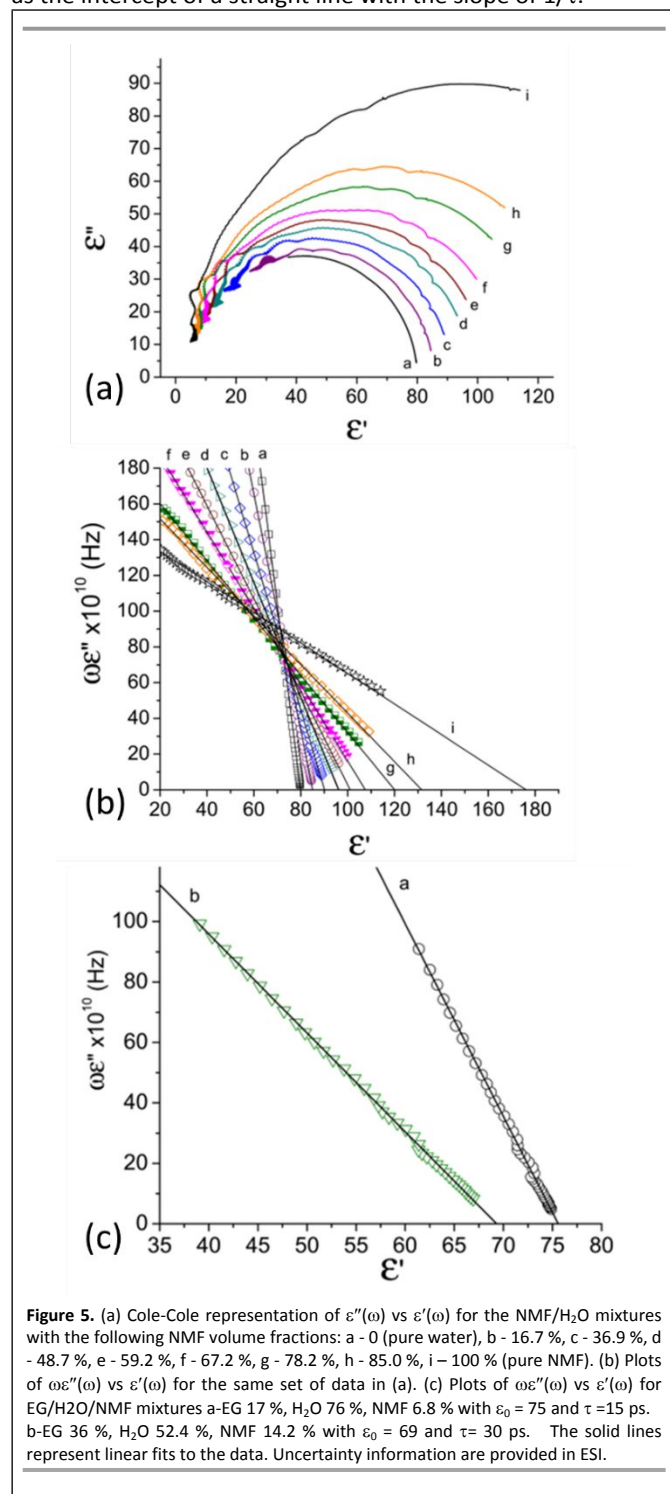


Figure 5b and 5c shows the plots of equation (3) for mixtures of NMF/H₂O and EG/NMF/H₂O, respectively, and the validity of equation (3). Results for EG/H₂O are shown in Section I, ESI. Linear regression was performed on 400 data points. For clarity,

only one symbol per 15 data points were plotted in Figures 5b and 5c. The presented fitted lines support our assumption behind equation (3), where the intercept of $\epsilon'(\omega) = \epsilon_0$ at $\omega = 0$ has the physical meaning of the static dielectric constant.

Laser Transmittance

The laser transmittance measurement was performed on a homemade setup that includes a 532 nm wavelength laser (Coherent VERDI), a set of neutral density filters, a sample heating stage with Quantum Northwest TC125 temperature controller, and a Thorlabs PM100D power meter. The KPSS-PDADMAB complex solutions were transferred into rectangular glass cuvettes and placed in the heating stage. The relative transmittance was obtained by normalizing the transmitted laser power of the sample by that of the empty cuvette. During a temperature scan, the samples were heated at a rate of 0.5 °C/min under constant stirring by a polytetrafluoroethylene stir bar, while the transmittance data as a function of time were recorded by the power meter software.

Dynamic Light Scattering (DLS)

The DLS measurements were performed on the same setup as described in the laser transmittance experiment, albeit with a photodiode detector equipped at the right angle (90°) to collect the scattered photon signals. Under the DLS mode, the scattered light intensities from filtered PEC samples as a function of time were monitored by the detector, recorded by the Brookhaven Windows 9kdlsw32 software, and simultaneously processed by a Brookhaven autocorrelator (TurboCorr) to give autocorrelation functions $g_2(\tau)$. This was then converted to the baseline-normalized first-order correlation function, $g_1(\tau)$, and fit to extract the decay rate Γ following the protocol described previously (Figure S10 and S11)²⁷. Finally, R_h were calculated using the Stokes-Einstein relationship assuming spherical particles: $R_h = kT/6\pi\eta_0D = kTq^2/6\pi\eta_0\Gamma$, where q is the scattering wavevector and $q = (4\pi n/\lambda)\sin(\theta/2)$ determined by the scattering angle (θ), the refractive index of the solvent (n), and the wavelength (λ) of the incident light in vacuum. The solvent viscosities (η_0) were estimated and provided in Figure S12.

Conflicts of interest

There are no conflicts to declare.

Acknowledgements

R.J.S.I. acknowledges partial support through the National Research Council-National Institute of Standards and Technology (NIST) Postdoctoral Fellowship Program. We acknowledge partial support from the NIST Materials Genome Initiative.

Notes and references

‡ Certain equipment, instruments, software, or materials are identified in this paper in order to adequately specify the experimental details. Such identification does not imply recommendation by the National Institute of Standards and Technology, nor does it imply the materials are necessarily the best available for the purpose.

The symbols M used to represent mol/L and are not in SI units, but used to adhere to the conventions of the Journal.

- 1 R. J. Stewart, C. S. Wang, I. T. Song and J. P. Jones, *Adv. Colloid Interface Sci.*, 2017, **239**, 88–96.
- 2 M. M. Feldstein, E. E. Dormidontova and A. R. Khokhlov, *Prog. Polym. Sci.*, 2015, **42**, 79–153.
- 3 K. Sadman, D. E. Delgado, Y. Won, Q. Wang, K. A. Gray and K. R. Shull, *ACS Applied Materials & Interfaces*, 2019, **11**, 16018–16026.
- 4 K. A. Black, D. Priftis, S. L. Perry, J. Yip, W. Y. Byun and M. Tirrell, *ACS Macro Lett.*, 2014, **3**, 1088–1091.
- 5 M. Muthukumar, *Macromolecules*, 2017, **50**, 9528–9560.
- 6 L. McQueen and D. Lai, *Front. Chem.*, 2019, **7**, 135.
- 7 H. Weingärtner, T. Merkel, U. Maurer, J.-P. Conzen, H. Glasbrenner and S. Käshammer, *Berichte der Bunsengesellschaft für physikalische Chemie*, 1991, **95**, 1579–1586.
- 8 N. C. Forero-Martinez, R. Cortes-Huerto, A. Benedetto and P. Ballone, *Molecules*, 2022, **27**, 1647.
- 9 J. Yu, N. E. Jackson, X. Xu, B. K. Brettmann, M. Ruths, J. J. de Pablo and M. Tirrell, *Science Advances*, 2017, **3**, eaao1497.
- 10 N. E. Jackson, B. K. Brettmann, V. Vishwanath, M. Tirrell and J. J. de Pablo, *ACS Macro Lett.*, 2017, **6**, 155–160.
- 11 H. Falahati and A. Haji-Akbari, *Soft Matter*, 2019, **15**, 1135–1154.
- 12 C. E. Sing and S. L. Perry, *Soft Matter*, 2020, **16**, 2885–2914.
- 13 J. Fu and J. B. Schlenoff, *J. Am. Chem. Soc.*, 2016, **138**, 980–990.
- 14 V. S. Rathee, H. Sidky, B. J. Sikora and J. K. Whitmer, *J. Am. Chem. Soc.*, 2018, **140**, 15319–15328.
- 15 F. G. Quiroz and A. Chilkoti, *Nature Materials*, 2015, **14**, 1164–1171.
- 16 G. L. Dignon, W. Zheng, Y. C. Kim and J. Mittal, *ACS Cent. Sci.*, 2019, **5**, 821–830.
- 17 G. L. Dignon, R. B. Best and J. Mittal, *Annual Review of Physical Chemistry*, 2020, **71**, 53–75.
- 18 S. Ali, M. Bleuel and V. M. Prabhu, *ACS Macro Lett.*, 2019, **8**, 289–293.
- 19 Y. Ma, S. Ali and V. M. Prabhu, *Macromolecules*, 2021, **54**, 11338–11350.
- 20 Z. Ye, S. Sun and P. Wu, *ACS Macro Lett.*, 2020, **9**, 974–979.
- 21 S. Adhikari, M. A. Leaf and M. Muthukumar, *The Journal of Chemical Physics*, 2018, **149**, 163308.
- 22 S. Adhikari, V. M. Prabhu and M. Muthukumar, *Macromolecules*, 2019, **52**, 6998–7004.
- 23 A. S. Ylitalo, C. Balzer, P. Zhang and Z.-G. Wang, *Macromolecules*, 2021, **54**, 11326–11337.
- 24 L. Li, A. M. Rumyantsev, S. Srivastava, S. Meng, J. J. de Pablo and M. V. Tirrell, *Macromolecules*, 2021, **54**, 105–114.
- 25 J. Lou, S. Friedowitz, J. Qin and Y. Xia, *ACS Cent. Sci.*, 2019, **5**, 549–557.
- 26 Q. Wang and J. B. Schlenoff, *Macromolecules*, 2014, **47**, 3108–3116.
- 27 Y. Ma, S. D. Hudson, P. F. Salipante, J. F. Douglas and V. M. Prabhu, *ACS Macro Lett.*, 2023, **12**, 288–294.
- 28 R. Chollakup, W. Smitthipong, C. D. Eisenbach and M. Tirrell, *Macromolecules*, 2010, **43**, 2518–2528.
- 29 D. Priftis and M. Tirrell, *Soft Matter*, 2012, **8**, 9396–9405.
- 30 D. Priftis, X. Xia, K. O. Margossian, S. L. Perry, L. Leon, J. Qin, J. J. de Pablo and M. Tirrell, *Macromolecules*, 2014, **47**, 3076–3085.
- 31 P. K. Jha, P. S. Desai, J. Li and R. G. Larson, *Polymers*, 2014, **6**, 1414–1436.
- 32 G. R. Leader and J. F. Gormley, *J. Am. Chem. Soc.*, 1951, **73**, 5731–5733.
- 33 S. J. Bass, W. I. Nathan, R. M. Meighan and R. H. Cole, *J. Phys. Chem.*, 1964, **68**, 509–515.
- 34 A. Sehgal and T. A. P. Seery, *Macromolecules*, 1998, **31**, 7340–7346.
- 35 S. K. Filippov, T. A. P. Seery, P. Černoč, J. Pánek and P. Štěpánek, *European Polymer Journal*, 2011, **47**, 1410–1415.
- 36 S. K. Filippov, T. A. Seery, J. Kříž, M. Hruby, P. Černoč, O. Sedláček, P. Kadlec, J. Pánek and P. Štěpánek, *Polymer International*, 2013, **62**, 1271–1276.
- 37 G. Akerlof, *J. Am. Chem. Soc.*, 1932, **54**, 4125–4139.
- 38 P. Zhang, N. M. Alsaifi, J. Wu and Z.-G. Wang, *The Journal of Chemical Physics*, 2018, **149**, 163303.
- 39 S. Meng, Y. Liu, J. Yeo, J. M. Ting and M. V. Tirrell, *Colloid Polym Sci*, 2020, **298**, 887–894.
- 40 C. M. Hansen, *Hansen Solubility Parameters: A User's Handbook, Second Edition*, CRC Press, Boca Raton, 2nd edn., 2007.
- 41 D. W. Van Krevelen and K. Te Nijenhuis, in *Properties of Polymers (Fourth Edition)*, Elsevier, Amsterdam, 2009, pp. 189–227.

- 42 T. Lindvig, M. L. Michelsen and G. M. Kontogeorgis, *Fluid Phase Equilibria*, 2002, **203**, 247–260.
- 43 I. Michaeli, J. Overbeek and M. Voorn, *Journal of Polymer Science*, 1957, **23**, 443–450.
- 44 D. Mukherji, C. M. Marques and K. Kremer, *Nat Commun*, 2014, **5**, 4882.
- 45 X. Zhang, J. Zong and D. Meng, *Soft Matter*, 2020, **16**, 7789–7796.
- 46 Y. Wei, P. Chiang and S. Sridhar, *The Journal of Chemical Physics*, 1992, **96**, 4569–4573.
- 47 Z.-G. Wang, *Phys. Rev. E*, 2010, **81**, 021501.
- 48 I. Nakamura, A.-C. Shi and Z.-G. Wang, *Phys. Rev. Lett.*, 2012, **109**, 257802.
- 49 C. E. Sing and M. Olvera de la Cruz, *ACS Macro Lett.*, 2014, **3**, 698–702.
- 50 M. G. Cacace, E. M. Landau and J. J. Ramsden, *Quarterly Reviews of Biophysics*, 1997, **30**, 241–277.
- 51 W. J. Xie and Y. Q. Gao, *J. Phys. Chem. Lett.*, 2013, **4**, 4247–4252.
- 52 M. Andreev, J. J. de Pablo, A. Chremos and J. F. Douglas, *J. Phys. Chem. B*, 2018, **122**, 4029–4034.
- 53 A. Salehi and R. G. Larson, *Macromolecules*, 2016, **49**, 9706–9719.
- 54 C. E. Sing, *Advances in Colloid and Interface Science*, 2017, **239**, 2–16.
- 55 C. E. Sing and J. Qin, *Macromolecules*, 2023, **56**, 5941–5963.
- 56 D. Jia, T. Zuo, S. Rogers, H. Cheng, B. Hammouda and C. C. Han, *Macromolecules*, 2016, **49**, 5152–5159.
- 57 D. Jia, M. Muthukumar, H. Cheng, C. C. Han and B. Hammouda, *Macromolecules*, 2017, **50**, 7291–7298.
- 58 R. A. Ferrell, *Phys. Rev. Lett.*, 1970, **24**, 1169–1172.
- 59 C. J. F. Böttcher, *Theory of electric polarization / Vol 2. Dielectrics in time-dependent fields*, Elsevier, Amsterdam ;, Second edition completely revised by O.C. Van Belle, P. Bordewijk, and A. Rip., 1978.

Data Availability Statement

The data supporting this article, including the calculation of the Flory-Huggins interaction parameters χ , the parameterization of Voorn-Overbeek model, and the measurement results of solvent dielectric constants and dynamic light scattering, have been included as part of the Supplementary Information.